Uppsala Dissertations from
the Faculty of Science and Technology
15

MARIA GUNTHER AXELSSON

Production Asymmetry of Strange Quarks in Electron–Positron Annihilation at LEP

ACTA UNIVERSITATIS UPSALIENSIS
UPPSALA 1998

Dissertation for the Degree of Doctor of Technology in High Energy Physics presented at Uppsala University in 1998

ABSTRACT

Gunther Axelsson, M. 1998: Production Asymmetry of Strange Quarks in Electron–Positron Annihilation at LEP. Acta Universitatis Upsaliensis, *Uppsala Dissertations from the Faculty of Science and Technology* 15. 150 pp. Uppsala. ISBN 91-554-4190-4.

The forward-backward asymmetry in the production of strange quarks in electron-positron annihilation has been measured at a centre-of-mass energy corresponding to the mass of the Z^0 particle. The asymmetry at this energy is highly sensitive to the ratio between the vector and axial-vector couplings of the quark to the Z^0 and to the value of the electroweak mixing angle $\sin^2\theta_W$. Together with the previously measured value of the forward-backward asymmetry of the bottom quark, the measurement provides a test of the important theoretical prediction that the couplings to the Z^0 are universal for all down-type quarks.

The analysis is based on 1.4 million hadronic Z^0 decays recorded in 1994 with the DELPHI detector system at the LEP collider at CERN. The strange quarks are selected using high-momentum charged kaons identified by the Ring Imaging CHerenkov (RICH) detectors. The charged kaon momentum is used to evaluate the probability for an event to belong to one of six possible event classes. Five classes are determined by the flavour of the primary quark (up, down, charm, strange and bottom) and the sixth class contains misidentified particles. The forward-backward asymmetry is determined using a maximum-likelihood method. At the Z^0 pole, the asymmetry is found to be

$$A_{\mathrm{FB}}^{0,s} = 0.105 \pm 0.016(\mathrm{stat.}) \pm 0.006(\mathrm{syst.})$$

which is the most precise measurement available for the strange quark asymmetry. The result is consistent with the previously measured value of the asymmetry of the bottom quark, and thus with the predicted universality of the down-type quark couplings to the Z^0. The obtained asymmetry corresponds to an electroweak mixing angle $\sin^2\theta_W = 0.2229 \pm 0.0030$.

Maria Gunther Axelsson, Department of Radiation Sciences,
Uppsala University, Box 535, S-751 21 Uppsala, Sweden.

ISSN 1104-2516
ISBN 91-554-4190-4

Distributor: Uppsala University Library, Uppsala, Sweden

To my father
Åke Gunther

Contents

Chapter 1

Introduction

Into something rich and strange.
William Shakespeare, *The Tempest*

The aim of elementary particle physics is to understand the behaviour and the interactions of elementary particles. The present knowledge in the field is formulated in the Standard Model which has proven to be a very powerful theory since its predictions are continuously being confirmed by experimental results. The validity of the model is tested in many ways at particle-physics laboratories around the world.

The Large Electron Positron collider (LEP) at the European particle-physics laboratory CERN near Geneva offers many possibilities of extensive tests of the theory. The analysis presented in this thesis is done using data collected at DELPHI (DEtector with Lepton, Photon and Hadron Identification), one of the four experiments at LEP.

One of the predictions of the Standard Model is that the creation of fermion-antifermion pairs in electron-positron annihilations is asymmetric: there is a larger probability for the fermion to be produced in the forward direction than in the backward direction, where the directions are defined by the electron beam. This so-called forward-backward asymmetry is explained by the fact that the weak force violates parity. The theory also states that the only features of the fermion that affects the asymmetry are its electric charge and weak isospin, and thus all fermions with the same charge and isospin (e.g. all down-type quarks) should have the same asymmetry.

The forward-backward asymmetries of the bottom and charm quarks have been measured to high precision by the LEP experiments. This thesis presents a measurement of the strange quark asymmetry. The analysis relies on the identification of fast hadrons containing strange quarks, which is possible at DELPHI since it is the only LEP experiment with RICH (Ring Imaging CHerenkov) detectors. DELPHI is therefore the experiment best suited for this kind of analysis. The aim of the study is to test the Standard Model prediction that the forward-backward asymmetry, and thus the coupling to the Z^0, is universal for down-type quarks.

In chapter 2, the theoretical background of the analysis is introduced (for a more thorough description, see for example [1, 2, 3]), and the forward-backward asymmetry is discussed in some detail. Chapter 3 presents the experimental setup of DELPHI, with some emphasis on the RICH detectors and the hadron identification. In chapter 4, the extraction of the forward-backward asymmetry of the strange quark with a maximum-likelihood method is described, and in chapter 5, the results are summarised and interpreted, and a comparison with other analyses is done.

Chapter 2

Theory

> *'Are you a physicist?'*
> *'Me?' said Johnny. 'I don't know anything about science!'*
> *'Marvellous! Ideal qualification!' said Einstein.*
> *'What?'*
> *'Ignorance is very important! It is an absolutely* essential *step in the learning process!'*
>
> Terry Pratchett, *Johnny and the Dead*

2.1 Introduction to the Standard Model

The Standard Model (SM) is a quantum-field-theoretical description of the elementary particles and the forces acting between them. It includes the strong interaction, electromagnetism and the weak interaction. The fourth fundamental force, gravity, is not included, since no quantum field theory of gravitation has yet been formulated. In the study of elementary-particle interactions, gravity can however be neglected since the gravitational force between individual particles is extremely weak.

In 1964, Gell-Mann [4] and Zweig [5] independently proposed hypothetical fundamental particles of three kinds (flavours): the up (u), down (d) and strange (s) quarks (q) (named by Gell-Mann), to describe the large number of different hadrons that had been observed experimentally. The hadrons were separated into two classes: baryons, containing three quarks (qqq), and mesons, consisting of a quark and an antiquark ($q\bar{q}$). To deal with problems of apparent violation of the Pauli exclusion principle in certain baryons, Greenberg [6] proposed the concept of colour charge for the quarks, commonly denoted red, green and blue. Hadrons, i.e. baryons and mesons, are postulated to be colourless. In baryons, the three quarks all carry different colour charge (red+green+blue = colourless), while in mesons the colour of the quark is cancelled by the anticolour of the antiquark. In hadrons, the quarks are held together through the exchange of so-called gluons (g_i, $i = 1, \ldots 8$). Quarks and gluons are often referred to as partons, and form the basic constituents of hadrons.

Later in the 1960s, Glashow [7], Salam [8] and Weinberg [9] formulated a field theory which combined the electromagnetic interaction, described by the Quantum Electrodynamic (QED) theory, with the weak interaction. The theory is generally called the standard electroweak theory or the GSW model. The theory successfully predicts the existence of three massive vector bosons: the Z^0, the W^+ and W^-, which mediate the weak force. They were detected experimentally in 1983 by the UA1 [10] and UA2 [11] collaborations at the CERN $p\bar{p}$ collider.

The development of the theory eventually led to the formulation of the Standard Model of particles and forces (gauge group $\mathrm{SU}(3)_c \otimes \mathrm{SU}(2)_L \otimes \mathrm{U}(1)_Y$). It uses two kinds of fundamental point-like particles: fermions (leptons and quarks) and bosons (Higgs, g_i, γ, $W^\pm$, Z^0). The forces are interpreted as an exchange of gauge bosons (g_i, γ, $W^\pm$, Z^0) between fermions. The strong interaction is described by Quantum Chromodynamics (QCD) and the electroweak interactions by the GSW model.

The masses of fermions and gauge bosons are attributed to the scalar Higgs boson (H^0) [12], which has not yet been observed experimentally. The Higgs mechanism is responsible for the spontaneous symmetry breaking of $\mathrm{SU}(2)_L \otimes \mathrm{U}(1)_Y$ to $\mathrm{U}(1)_Q$, the gauge group of QED. If this is done by the simplest mechanism, the result is three massive vector bosons ($W^\pm$, Z^0) and one Higgs scalar. The charged weak current ($W^\pm$) is purely associated with $\mathrm{SU}(2)_L$, while the neutral currents from $\mathrm{U}(1)_Y$ and $\mathrm{SU}(2)_L$ undergo mixing, which produces a massless photon and a massive Z^0 boson. The strength of the mixing is given by the weak mixing angle θ_W, also called the Weinberg angle, which is a free parameter of the theory and has to be determined from experiment. The weak mixing angle can, following the definition introduced by Sirlin [13], be written as

$$\sin^2\theta_W = 1 - \frac{M_W^2}{M_Z^2}, \tag{2.1}$$

where M_W and M_Z are the masses of the $W^\pm$ and Z^0. The unbroken

	interaction		
	strong	electroweak	gravity
gauge bosons	$g_1 \dots g_8$	γ, $W^{\pm}$, Z^0	graviton?
theory	QCD	GSW	general relativity
gauge group	SU(3)	$\mathrm{SU}(2) \otimes \mathrm{U}(1)$	?
masses	0	$0, M_W, M_Z$	0
charge	colour	weak isospin, weak hypercharge	mass
coupling	α_s	g, g'	G

Table 2.1. *The fundamental interactions and some of their characteristics.*

symmetry $\mathrm{SU}(3)_c$ accounts for the gluon field, with eight different colour states. An overview of the gauge bosons and the fundamental forces are found in table 2.1. α_s is the strong coupling constant, and g and g' are the electroweak coupling constants, related through $g \sin\theta_W = g' \cos\theta_W = e$.

The fundamental fermions (quarks and leptons), the basic constituents of matter, can be separated into three generations of families with left-handed doublets and right-handed singlets (the left- and right-handedness, or the chirality, is defined by the chiral operator $\frac{1}{2}(1 \mp \gamma_5)$, where γ_5 is a product of the Dirac matrices: $\gamma_5 = i\gamma^0\gamma^1\gamma^2\gamma^3$. It is equivalent to the helicity for mass-less fermions). Table 2.2 shows the fermion families and their electroweak quantum numbers: the weak isospin I, its third component I_3 and the weak hypercharge Y. The electric charge of a fermion is given by the Gell-Mann-Nishijima relation

$$Q = I_3 + \frac{Y}{2}.$$

In addition, quarks carry colour charge while leptons do not. As a consequence, the strong force only acts on quarks. The number of generations (three) is not determined by the theory but by experimental observations.

Quark flavour is conserved by the strong interaction (QCD) but not in the GSW model since the charged weak current is flavour changing. The quark mass eigenstates are therefore not the same as the weak eigenstates. The weak eigenstates d', s', b' of charge $-\frac{1}{3}$ in table 2.2 are related to the mass eigenstates d, s, b through the Cabibbo-Kobayashi-Maskawa (CKM) mixing matrix [14]. Each element in the matrix represent a cou-

Fundamental fermion families			Quantum numbers			
1st	2nd	3rd	I	I_3	Y	Q
$\begin{pmatrix}\nu_e\\ e\end{pmatrix}_L$	$\begin{pmatrix}\nu_\mu\\ \mu\end{pmatrix}_L$	$\begin{pmatrix}\nu_\tau\\ \tau\end{pmatrix}_L$	$\frac{1}{2}$	$+\frac{1}{2}$ $-\frac{1}{2}$	-1 -1	0 -1
e_R	μ_R	τ_R	0	0	-2	-1
$\begin{pmatrix}u\\ d'\end{pmatrix}_L$	$\begin{pmatrix}c\\ s'\end{pmatrix}_L$	$\begin{pmatrix}t\\ b'\end{pmatrix}_L$	$\frac{1}{2}$	$+\frac{1}{2}$ $-\frac{1}{2}$	$+\frac{1}{3}$ $+\frac{1}{3}$	$+\frac{2}{3}$ $-\frac{1}{3}$
u_R	c_R	t_R	0	0	$+\frac{4}{3}$	$+\frac{2}{3}$
d_R	s_R	b_R	0	0	$-\frac{2}{3}$	$-\frac{1}{3}$

Table 2.2. *The quantum numbers of the leptons and the quarks. The quarks, up (u), down (d), charm (c), strange (s), top (t) and bottom (b) also carry colour charge. The leptons are the electron (e), the muon (μ) and the tau (τ) and the corresponding neutrinos (ν_e, ν_μ, ν_τ). The quarks d', s' and b' are obtained from the mass eigenstates d, s and b through the CKM matrix (see text).*

pling of a quark of charge $+\frac{2}{3}$ to a quark of charge $-\frac{1}{3}$. By convention, up-type quarks are left unmixed.

The weak force violates parity (space-inversion symmetry) and has different couplings to fermions of different chirality. As mentioned above, the charged weak current is associated purely with $\mathrm{SU}(2)_L$. The index L refers to left-handed, indicating that only left(right)-handed fermions (antifermions) couple to $W^{\pm}$. The mixing of $\mathrm{U}(1)_Y$ and $\mathrm{SU}(2)_L$ neutral gauge bosons, which gives rise to the photon and the Z^0 boson, results in different couplings of the Z^0 for left- and right-handed fermions. This is the origin of the forward-backward asymmetry, which will be discussed in more detail below. Right-handed neutrinos (and left-handed antineutrinos) completely decouple from all other fermions in the Standard Model, and have never been observed.

The mediators of the strong force, the gluons, carry colour charge, and thus they interact strongly with each other. Quarks and gluons have never been observed as free particles. This fact is explained by the concept of confinement, which states that quarks are only found in colourless bound states (hadrons). The value of the QCD coupling constant α_s depends on the squared four-momentum transfer Q^2 of the interaction process (this is called the running of α_s). The confinement of the quarks is explained by the sharp increase of α_s for small values of Q^2 (i.e. increasing distance). For $Q^2 \rightarrow \infty$, on the other hand, α_s vanishes. The interpretation of this is that quarks can be considered as free or very weakly interacting at small distances (as in hadrons), they achieve so-called asymptotic freedom. The exact behaviour of α_s is often described in terms of the parameter Λ_{QCD}, which has to be determined from experiment.

Since the theoretical formulation of the Standard Model, its predictions have been tested by a large number of experiments. In the first phase of the LEP collider (LEP1, 1989-1995), the electrons and positrons collided at energies very close to the Z^0 mass, and thus acted as a Z^0 factory. Several million Z^0 decays were produced in LEP1, and extensive precision tests of the theory have been performed. Even more aspects can be studied at the present second phase of the collider (LEP2), where the centre-of-mass energy is well above the threshold for $W^\pm$ pair production.

2.2 Physics of e^+e^- annihilation

The electroweak interaction is studied at LEP through the reaction

$$e^+e^- \rightarrow f\bar{f}$$

i.e. electron-positron annihilation producing a fermion-antifermion pair. If the created particles are a quark and an antiquark (so-called hadronic e^+e^- annihilation), the final state particles are formed through a sequence of separate phases, as illustrated in figure 2.1:

1. The formation of a quark-antiquark pair through a virtual gauge boson. This process is described by the GSW model. Real photons can be radiated from the initial e^+e^- state and from the final $q\bar{q}$ state. These so-called bremsstrahlung effects are described by QED.

2. The radiation of hard gluons from the final-state quarks. This process can be calculated numerically beyond lowest order in α_s using perturbative QCD. Two approaches can be used: the QCD matrix element (ME) calculations (up to second order in α_s), or

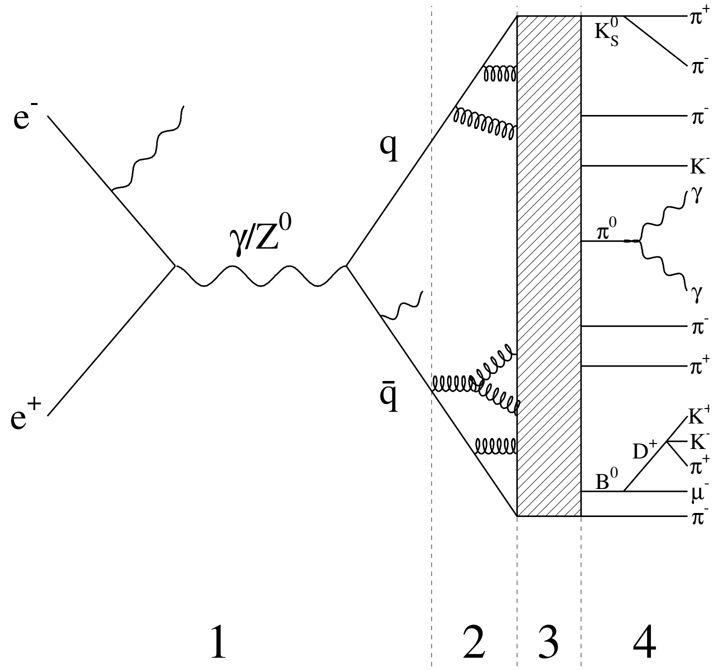

Figure 2.1. Schematic illustration of the four phases of a hadronic e^+e^- annihilation: (1) electroweak phase with initial and final state photon radiation, (2) perturbative QCD phase with gluon radiation, (3) non-perturbative fragmentation phase, and (4) decays of final state particles.

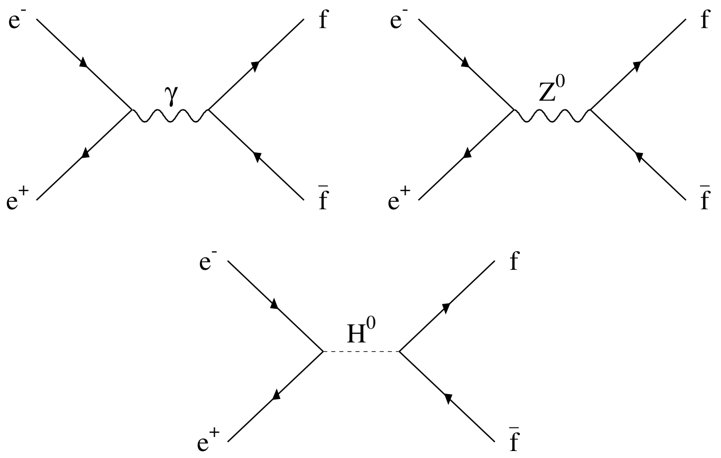

Figure 2.2. The lowest order Feynman diagrams for $e^+e^- \to f\bar{f}$

the parton shower (PS) model with a leading logarithm approximation (LLA). ME can only be used for final states with up to four partons.

3. The fragmentation of quarks and gluons into hadrons. No perturbative calculations are possible in this phase, so the description of it must rely on phenomenological fragmentation models, as will be described in section 2.4.

4. The decay of unstable particles produced in the fragmentation of the quarks into final-state leptons, photons and hadrons that can be detected in particle physics experiments.

The first phase, the creation of a fermion-antifermion pair, will be discussed in this section.

The three lowest order Feynman diagrams for $e^+e^- \to f\bar{f}$ when $f \neq e$ are shown in figure 2.2, corresponding to a virtual photon (γ), a virtual Z^0 and a virtual Higgs boson. For $f = e$ (Bhabha scattering) there are three additional diagrams due to the possibility of both space-like (s-channel) and time-like (t-channel) exchange of the virtual bosons. Only the processes with $f \neq e$ will be treated here. The third diagram will only contribute at centre-of-mass energies close to the mass of the Higgs boson, and, due to the smallness of the coupling to $e^\pm$, can be neglected even if $M_H \cong M_Z$.

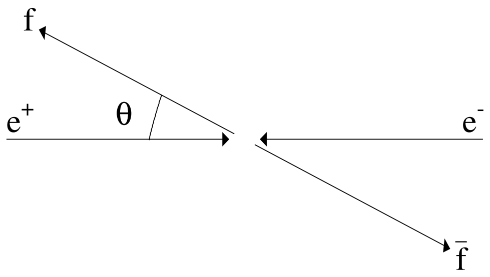

Figure 2.3. The geometry of the reaction $e^+e^- \rightarrow f\bar{f}$.

Defining the angle θ as the angle between the directions of the incoming electron and the produced fermion as in figure 2.3, the differential cross section of the process can be written as [15]

$$\frac{\mathrm{d}\sigma}{\mathrm{d}\Omega} = \frac{\alpha^2}{4s} N_f \beta_f \left\{ G_1(s)(1+\cos^2\theta) + \beta_f G_2(s) 2\cos\theta + 4\mu_f G_3(s)\sin^2\theta \right\}, \tag{2.2}$$

where Ω is the solid angle, α is the fine structure constant, s is the squared centre-of-mass energy, N_f is the number of possible colour states of the final fermion (3 for quarks, 1 for leptons), and $\beta_f = \sqrt{1-4\mu_f}$, where $\mu_f = m_f^2/s$ is the squared reduced mass of the fermion. The functions G_i are given by

$$\begin{aligned}
G_1 = {} & Q_e^2 Q_f^2 + 2Q_e Q_f g_V^e g_V^f \mathrm{Re}F + [(g_V^e)^2 + (g_A^e)^2][(g_V^f)^2 + (g_A^f)^2\beta_f^2]|F|^2 \\
G_2 = {} & 2Q_e Q_f g_A^e g_A^f \mathrm{Re}F + 4 g_V^e g_A^e g_V^f g_A^f |F|^2 \\
G_3 = {} & Q_e^2 Q_f^2 + 2Q_e Q_f g_V^e g_V^f \mathrm{Re}F + [(g_V^e)^2 + (g_A^e)^2](g_V^f)^2 |F|^2 .
\end{aligned} \tag{2.3}$$

Q_e and Q_f are the charges of the electron and the fermion, and $g_V^{e(f)}$ and $g_A^{e(f)}$ are the vector and axial-vector couplings of the electron (fermion) to the neutral current. The neutral-current couplings for left-handed and right-handed fermions (also for $f = e$) are given by

$$\begin{aligned}
g_L^f &= I_3^f - Q_f \sin^2\theta_W \\
g_R^f &= -Q_f \sin^2\theta_W ,
\end{aligned}$$

and g_V^f and g_A^f are obtained from

$$\begin{aligned}
g_V^f &= g_L^f + g_R^f &= I_3^f - 2Q_f \sin^2\theta_W \\
g_A^f &= g_L^f - g_R^f &= I_3^f .
\end{aligned}$$

The function $F = \eta\chi_0(s)$ is a product of the Z^0 propagator

$$\chi_0(s) = \frac{-s}{s - M_Z^2 + iM_Z\Gamma_Z}, \tag{2.4}$$

where M_Z and Γ_Z are the mass and the width of Z^0, and the normalisation factor

$$\eta = \frac{1}{(2\sin\theta_W\cos\theta_W)^2}. \tag{2.5}$$

Close to the Z^0 peak, μ_f is very small, even for b quarks ($\mu_b \approx 0.003$) and thus the differential cross section can be approximated by

$$\frac{\mathrm{d}\sigma}{\mathrm{d}\Omega} = \frac{\alpha^2}{4s}N_f G_1(s)\{(1+\cos^2\theta) + \frac{G_2(s)}{G_1(s)}2\cos\theta\}.$$

For pure γ exchange (pure QED processes) $G_1 = Q_e^2 Q_f^2$ and $G_2 = 0$, giving

$$\left.\frac{\mathrm{d}\sigma}{\mathrm{d}\Omega}\right|_{\mathrm{QED}} = \frac{\alpha^2 N_f Q_e^2 Q_f^2}{4s}(1+\cos^2\theta)$$

which is symmetric in $\cos\theta$. Adding Z^0 exchange introduces the strongly energy-dependent asymmetric term $[G_2(s)/G_1(s)]2\cos\theta$, which leads to the forward-backward asymmetry.

2.3 The forward-backward asymmetry

2.3.1 Definitions

The forward-backward asymmetry of the process $e^+e^- \to f\bar{f}$ is defined by

$$A_{\mathrm{FB}}^{f\bar{f}} \equiv \frac{\sigma_F^f - \sigma_B^f}{\sigma_F^f + \sigma_B^f}$$

where $F(B)$ denotes the forward (backward) region defined by $\cos\theta > 0$ (< 0) and with θ defined as in figure 2.3, so that the cross sections $\sigma_{F(B)}^f$ are given by

$$\begin{aligned} \sigma_F^f &= 2\pi \int_0^1 \frac{\mathrm{d}\sigma^f}{\mathrm{d}\Omega}\mathrm{d}(\cos\theta) \\ \sigma_B^f &= 2\pi \int_{-1}^0 \frac{\mathrm{d}\sigma^f}{\mathrm{d}\Omega}\mathrm{d}(\cos\theta) \quad . \end{aligned}$$

Using equation (2.2), the asymmetry can be written as

$$A_{\mathrm{FB}}^{f\bar{f}}(s) = \frac{3}{4}\frac{G_2(s)}{G_1(s) + 2\mu_f G_3(s)}\sqrt{1 - 4\mu_f}.$$

Neglecting the fermion masses ($\mu_f \approx 0$), this becomes

$$A_{\mathrm{FB}}^{f\bar{f}}(s) = \frac{3\,G_2(s)}{4\,G_1(s)},$$

so the differential cross section can be expressed as

$$\frac{\mathrm{d}\sigma}{\mathrm{d}\Omega}(s,\theta) = \frac{\alpha^2}{4s}N_f G_1(s)\{(1+\cos^2\theta) + \frac{8}{3}A_{\mathrm{FB}}^{f\bar{f}}(s)\cos\theta\}. \tag{2.6}$$

The differential asymmetry $\mathcal{A}$, or the forward-backward asymmetry at a given angle θ, is given by

$$\mathcal{A}(s,\theta) = \frac{\frac{\mathrm{d}\sigma}{\mathrm{d}\Omega}(s,\theta) - \frac{\mathrm{d}\sigma}{\mathrm{d}\Omega}(s,\pi-\theta)}{\frac{\mathrm{d}\sigma}{\mathrm{d}\Omega}(s,\theta) + \frac{\mathrm{d}\sigma}{\mathrm{d}\Omega}(s,\pi-\theta)}.$$

Inserting $\frac{\mathrm{d}\sigma}{\mathrm{d}\Omega}$ from equation (2.6) gives

$$\mathcal{A}(s,\theta) = \frac{8}{3}A_{\mathrm{FB}}^{f\bar{f}}(s)\frac{\cos\theta}{1+\cos^2\theta}.$$

In figure 2.4, the energy dependence of the asymmetries in the Born approximation is shown. Close to the Z^0 mass, the asymmetry increases rapidly with $\sqrt{s}$, while the energy dependence decreases as the Z^0 exchange becomes less dominant.

2.3.2 The asymmetry near the Z^0 pole

At the Z^0 pole $\sqrt{s} = M_Z$ and the propagator $\chi_0(s)$ of equation (2.4) becomes purely imaginary. Thus, the terms in equation (2.3) proportional to $\mathrm{Re}\chi_0(s)$ vanish. This leaves the pure QED terms, proportional to $Q_e^2 Q_f^2$, and the Z^0 exchange terms, proportional to

$$|\chi_0(s = M_Z^2)|^2 = \frac{M_Z^2}{\Gamma_Z^2},$$

while the γ-Z^0 interference terms disappear. The QED terms are completely dominated by the Z^0 exchange terms. As a consequence, the

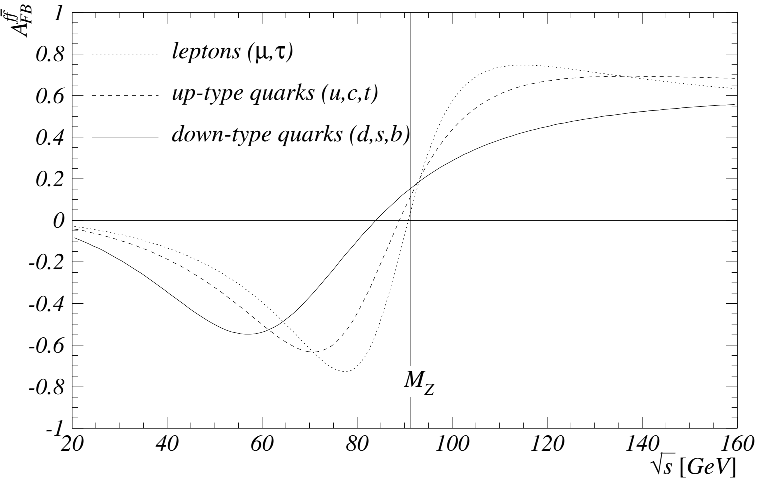

Figure 2.4. Born-level asymmetries as a function of the centre-of-mass energy.

Born level asymmetries at the Z^0 pole can be expressed in terms of the coupling constants of the fundamental fermions to the Z^0 through the relation

$$A_{\mathrm{FB}}^{0,f} = A_{\mathrm{FB}}^{f\bar{f}}(M_Z^2) = \frac{3}{4}\mathrm{Z0\Gamma sd\Gamma 402855Fo{-}m\Gamma dup\Gamma 0\Gamma eo{-}m\Gamma dup199\Gamma X\Omega\Gamma s\Gamma[]\Gamma 0\Gamma s}$$

Figure 2.10. illustration of (a) the string fragmentation model and (b) Ancluster fragmentation mo

whichthencontinuetofragmentindependentlyintheirown
censystemsuntilonlyboundhadronstatesremain. Barytre-of-massare produced through direct producti

inhadrons. particle momentum distributions are determined from
the momenta and decay properties of the parent The fragmentation models are implemented in

[redacted]

where $p^{\perp}$ is the transverse momentum with respect to the quark tion, and z is given by

$$z \; (E + _{\parallel} \qquad ^{hadron} \quad (E + p = _{quark}$$

where E is the energy and $_{\parallel}$ is the momentum component parallel to quark direction. Fthe heavier c

function, called the Peterson function [27] is commonly used:

$$f(z) \; 1\alpha \left(1 - \frac{1}{-} \; \frac{\varepsilon}{1-z} \right) \quad \text{where} \; _q$$

is a parameter to be determined from experiment.

transverse momenta of the hadrons are determined from the transverse momenta of their constituent quarks. The distribution of is gaussian, and its standard dev

parameter.

The flavours of the generated $q\bar{}$pairs are determined from a tion proportional to $\exp(-m$ ^{q}) that suppresses heavy quark production probability of production of different quark flavours are given by The $P($

d: $P(s\bar{s}$: $P(c\bar{c}$ = γ $\beta\gamma$ $d\,\gamma$ $\beta\gamma$ β 0.3 1 : 1 The meson production is determined by

the created particles can be any of the six lightest multiplets. With L denoting the orbital angular momentum, S the spin and J = $L + S$ the total angular momentum, and using the notation ^{2ss}

Heaeventscanbeidentifiedfromsemi-leptonicdecaysof
heavyhadrons,givingpromptleptonswithhigh,especiallyfor$p$quarks.longlifetimesandlargemassesofBha

these tags, the LEP experiments have been able to measure the pasymmetries of b and c with high pre

$$\begin{aligned} A^{0\mathrm{FB}} &= 0.0983 \pm 0.0024 \\ A_{\mathrm{FB}}^{0,c} &= 0.0739 \pm 0.0048. \end{aligned}$$

To tag events with primary s quarks is more difficult, since s can be produced during the fragment

$s\bar{s}$thereforbemeasuredcanThe measurement of A
$s$provides the first test of universality of the down-type quark

the Standard Model (section 2.2). main motivation for this sis is thus to investigate if the down-t

precisely the asymmetries of the b and s quarks, are equal, as the theory
predicts.

ChapterThe DELPHI experimen*And if thou doubt me, first to Delphi There ascerta*

Sophocles, *Oedipus the King*

The DELPHI detector has been in operation at the LEP + e^- lider at CERN since was designed

The experiment is described in detail in [29a description its main features will be given. The id

will be discussed in some detail, since it is of great importance to present of

The LEP collide

The Large Electron Positron collider (LEP) at CERN is an e^+e^- 3.1with a circumference of 26.6 km. f

in LEP in July 1989, and in August the same year the first between electrons and positr

energy × 45.6 GeV = 91.2 (2In total, about 4 million hadronic
decays have been recorded at
[30]. 1995 and 1996, LEP was upgraded to its Duringphase, LEP2, with a higher beam energy.

LEP2 is running at energies above the ± threshold.

There are four experiments at **ALEPH** Apparatus for LEP **DELPHI** with Lepton, Photon an

the electron and positron bexperiments are built and run
by collaborations of several hundred physicists from universities Thelaboratories all over the world

The analysis presented in this thesis is based on data collected eams.DELPHI during phase on

ΛΛΛΛΛ

Figure 3.1. Schematic layout of

[redacted]solution detector$r$ [cm] $|z|$ [cm] θ [deg]σ

[redacted]

[redacted]

$r\phi$ σVD6.3/9.0/10.9 0.009 (28-152)ID

MUS530-640 - Table 3.1. *Geometrical coverage and resolutions of the DELPHI tracking -tectors*

vertex detector for measurements of tracks close to the interaction poinIt consists of three coaxial cylin thebeamdirection. two outer layers are 24 cm long, the innermost layer was increased to 27 cm in 1994, thus

Tracwith polar angles of $\circ$ $\leq \theta \leq$ −−−cross all three laySince 1994, the

–cross a volume sensed by at least 10 Each of the five MWPC layers has 192 a

beam axis and 192 circular cathode strips giving rz information. wires.information from the MWP

depending on θ, for an isolated trac5**Time Projection Chamber** The time projection chamber is t

by

a high-tension plate. The two end-plates are divided into six azimffisectors with 192 sense wires and

The single-point resolutions of the TPC are r= 250 μm and r880 μ**Outer Detector ff**Since the size of the TPC i

of the drift-tube layers provide fast z information by relative timing the signals from both The single

bers. It consists of two layers: layer is inserted into the return yokof the magnet after 90 cm of ir

the length of a yoke sector, with clearance between them for of cables and pipes. Each plank cont

chambers (both planes are read out). All chambers are operated in passageproportional moThe resol

Forward Chamber A (F The tracking detectors in the forward (endcap) regions are the forwchambers A and F

, thus providing three coffi(x, u, v) measured twice owing to the

= 240 μy= 8.5 mrad, and = 24 mrad (aver

The resolutions achieved in the detector are β= 150 μm, 3.mrad, and = 4.0/$\sin\theta$ **Forward M**

and composed

of four quadranA quadrant contains two orthogonal layers of 22 drift
chambers, operated in the limited streamer mo**Surround Muon Chambers ts.**The surround muon

At each endcap there are four stations, on the sides, top and bof DELPHI. A station consists of two modules of

are inclined by about m∘ in order to be orthogonal to tracks from interaction region. The modules

thus providing two coordinates. The intrinsic resolutions about 2.5 cm and 1 cm respectively [33].

has a good time stability and provides a long lever arm with respareto the interaction point. Ass

track, the position of the VD with respect to the OD can be The ID and TPC can then be aligned fro

–(GeV/c3–and the wider Gaussian, which has a peak value of a

(GeV/c)$^{-1}$The corresponding distribution for muon tracks in the forw

detected at least in the innermost layer of the VD and in FCB has .standard deviation $\sigma(1/p) = 1$

–(GeV/c) –.

[redacted]

(/) [(GeV/c−1

[redacted]

≥ VD+ID+TPC+OD 0.6 × 42–≥

–FCB 1.5 × included–< FCB 2.7 × 10

–Table 3.2. *Momentum measurement resolutions f*

In table 3.2, the momentum resolutions for dimuons in different of the detector and with different com

$\leq \theta \leq 150$), but deteriorate in the forward of the In DELPHI there are four el

hadronic: HCAL. The STIC, SAT and VSAT are mainly used theluminosity measurements an

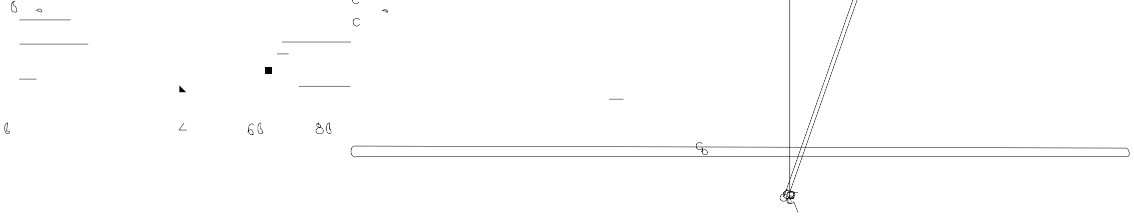

Figure 3.2. Resolutions of the track coordinates obtained by comparing simu-
lated and reconstructed parameters: (a) momentum resolution as a function the polar angle θ, (b) momentum re

of θ, (d) azimuthal angle resolution as a function of the momentum for tracks, (e) polar angle resolution as a

[redacted]

EVSAT 6-8 770-780 0.3-0.4 24 X

EE[cm] $|z|$ [cm] [deg]

$4.3 + {}^{32}\surd$

EHCAL b [redacted]

= 0.0430.

where E is given in GeV. The angular resolutions for high energy photons

11.E

0 $\surd$ +2.3

STIC 0

o5 at 45 GeVTable 3.3. *Geometrical coverage and ene*

SAT 10-36 233-285 2

PHI calorimeters. The depth of the electromagnetic calorimeters is given in
radiation lengths (), and for the hadronic calorimeters it is given in nucleabsorption lengths (λ). The STIC rep

high density material in the gas volume. The layers are made of lead and servboth as converter material and for providing the drift field. total depth of the calorimeter is 18sin

[redacted]ngth. The ionization electrons deposited by electromagnetic showparticles in the gas gaps betwee

counters with a two-dimensional readout. The third spatial coordinate is given by the drift time. A plane of scintillators is inserted into one of the gas gaps at a depth of about 4.5 radiation lengths to provide The relative resolution in the me

$\sigma(E)$ EFEMC 40-227 284-324

1.2

are ±1.7 mrad in ϕ and ±1.0 mrad in θ.

Forward Electromagnetic Calorimeter (FEMC)

The forward electromagnetic calorimeter is a lead glass calorimeter. It consists of two 5 m diameter disks; one in each endcap of The disks contain 4532 Cherenkov lead

faces at $|z| = 284$ cm, and cover polar angles of $8^\circ < \theta < 35^{145}$
$< \theta < 172$ ° respectively. The blocks are truncated pyramids with
a depth of 40 cm, corresponding to 20 radiation lengths, and they arranged to point close to the in

E

$$= 0.03 + \overset{0.12}{+} \quad 0.11$$

with E in GeV.

Hadron Calorimeter (HCAL)

The hadron calorimeter is a sampling gas detector installed in the yoke of the DELPHI solenoid. It has

. The detector

consists of streamer tubes, operating in the limited streamer mode, 18 mm wide slots between 50 m

of tubes and plates in the barrel and 19 layers in each endcap. In barrel, the energy resolution of t

1.12 with E in GeV.

3.2.3 RICH

As mentioned, DELPHI was designed to be a detector with powerful

particle identification over a large momentum range. To meet requirements, large-scale ring imag

distinguishes DELPHI from the other LEP experimenThe RICH technique is based on the Cher

charged particle traverses a dielectric medium at a velocity larger than the velocity of light in the medium, it produces a cone of Cherenkov light. The emission angle of the light, θ, is given by

$$\cos\theta_C = \frac{1}{\beta n} \quad (3.1)$$

where β is the velocity of the particle and n is the refractive index the medium. Since

$$\frac{1}{\beta^2} = \sqrt{}^{2} + 1$$

where m and p are the rest mass and the momentum of th

$$m = p\Lambda\cos{}^2\theta_C - 1. \qquad (3.2)$$

Thus, the Cherenkov angle together with the momentum of the (measured by the tracking detectors)

This information is also used for identification of particles; so-called idenThe number of emitted Cherenkov photons N with energies in the interval E to $E +$ is given by the relation [19$_{ph}$

Z α ${}^2]_2$ $dE$where α is the electromagnetic fine-structure constan

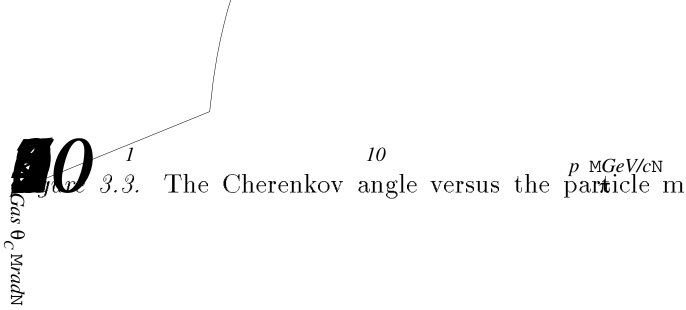

gure 3.3. The Cherenkov angle versus the particle momentum for pions,

kaons and protons for the Barrel RICH liquid and gas photons for particle identification. Fequation (3.1

1, which

implies that a dense radiator medium will detect slower particles than a thin There are two RICH detectors at DELPHI: the Barrel RICH (BRICH)

and the Forward RICH (FRICH) [35]. They use one liquid (n, = 1.2718) and one gaseous (5 12 , n = 1.001941 in BRICH; 4, n = 1.001512 in FRICH) radiator. The gaseous radiator of the Barrel RICH is kept at constant pressure (1030 mbar) and temperature C∘ C) in order to prevent condensation (the boiling point of Λis 28 and to provide stable operation. In

and the pressure of the gaseous radiator are allowed to vary (the bing point of 4 10 is −1.7° C), but their values are carefully monitored.
4 10 is not used in the Barrel RICH since the particle tracks would generate enough Cherenkov photo

a thin medium (the gas volume traversed by the particle tracks is shorter in the Barrel RICH than in the Forward RICH). Figure 3.3 shows Cherenkov angle versus the part

Figure 3.4. Longitudinal cross section of a quarter of the Barrel RICH.

in the Barrel RICH. The liquid radiator provides separation of more than 2σ of kaons and pions in the momentum range from 0.8 GeV/c to 3 GeV/c (where σ is the width of the Cherenkov angle distribution), and the gas radiator of the Barrel (Forward) RICH separates kaons and pions between 2.5 (2.7) GeV/c and 20 (22) GeV/c.

The layout of the Barrel RICH is shown in figure 3.4. It is a 3.5 m long cylinder with inner and outer radii of 123 cm and 197 cm respectively. The cylinder is divided into two halves by a central support wall and azimuthally into 24 sectors. Each sector contains a liquid radiator box close to the inner radius with 1 cm of liquid, a photon detector, a gas volume and 6 parabolic mirrors. The mirrors are used to reflect and focus the photons emitted in the gas volume, so the photons produced in both radiators are detected by the same photon detector. The photon detector consists of a drift-tube with a drift gas of 75% CH_4 and 25% C_2H_6, and with Tetrakis-diMethyl-Amino-Ethylene (TMAE) as photo-ionizing agent. The drift-tube acts as a time projection chamber (TPC) with multiwire proportional chambers (MWPCs) for readout at the outer end. The liquid radiator boxes and the photon detectors have fused quartz windows with a transparency close to the transparency of the radiators, and photons with wavelengths in the range 170 to 220 nm (UV photons) are detected with high efficiency. The Barrel RICH has been fully operational since 1992.

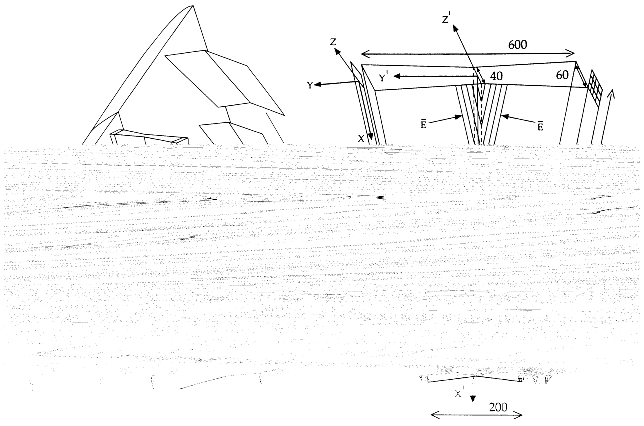

Figure 3.5. Left: a sector of the Forward RICH; 1 = liquid radiator containers, 2 = mirrors, and 3 = TPC-unit. Right: schematic view of the TPC-unit [36].

The Forward RICH has a different design because of the geometry of DELPHI. It is installed at 172 cm $< |z| <$ 266 cm and has an inner radius of 45 cm and an outer radius of 125 (180) cm at the face closest to (furthest from) the interaction point. Azimuthally it is divided into 12 sectors. The design of a sector is shown in figure 3.5. It has three liquid radiator containers, one TPC-unit (drift gas: C_2H_6 + TMAE) with two MWPCs, and five spherical mirrors. The drift field in the TPC-unit is divided in two uniform halves (see figure 3.5). In both cases the electric drift field is perpendicular to the external magnetic field, resulting in a Lorentz angle of about 50° with respect to the electric field. The Forward RICH has been fully operational since 1994.

The identification of particles in the RICH detectors relies on the resolution in the Cherenkov angle. This resolution is mainly determined by the uncertainty in the photon conversion point, which depends on errors in the tracking and on the granularity of the detector: the anode-wire pitch (2.62 mm), the cathode-strip pitch (4 and 5 mm for Barrel and Forward RICH respectively), and the drift time resolution (10 ns). There is also an uncertainty in the conversion point due to electron diffusion, which varies between 1 and 3 mm, depending on the drift distance. Table 3.4 shows the average precisions for single photoelectrons and for tracks measured in $Z^0 \to \mu^+\mu^-$ events. In order to obtain the best possible resolution in Cherenkov angle, precise knowledge of the positions

liquid radiator	Barrel	Forward
Number of photoelectrons per track	14	7
Cherenkov angle [mrad]	666	675
Angular precision per photoelectron [mrad]	13.3	11.4
Angular precision per track [mrad]	5.2	5.0
gas radiator		
Number of photoelectrons per track	8	8
Cherenkov angle [mrad]	62.3	55.0
Angular precision per photoelectron [mrad]	4.3	2.5
Angular precision per track [mrad]	1.5	1.2

Table 3.4. *Number of photoelectrons, Cherenkov angle and precision (in mrad) measured in* $Z^0 \rightarrow \mu^+\mu^-$ *events, for the Barrel and Forward RICH [30].*

of the radiators, detectors and mirrors as well as of the refractive indices is crucial. Since direct measurements of these parameters are not sufficient, an off-line alignment based on real data is needed. This alignment is described in detail in [37] together with a thorough descripo(ks)ta i1Γb(4.3)135Ωb(2.5)pΓ1593Γ950